


# Microsolvation of $\text{Sr}^{2+}$ , $\text{Ba}^{2+}$ : Structures, energies, bonding, and nuclear magnetic shieldings

Angie Velásquez<sup>1</sup> | Yuly Chamorro<sup>1,2</sup> | Alejandro Maldonado<sup>3</sup>  |  
Gustavo Aucar<sup>3</sup>  | Albeiro Restrepo<sup>1</sup> 

<sup>1</sup>Instituto de Química, Universidad de Antioquia UdeA, calle 70 No 52-21, Medellín, Colombia

<sup>2</sup>Van Swinderen Institute for Particle Physics and Gravity, University of Groningen, Groningen, The Netherlands

<sup>3</sup>Department of Physics, Natural and Exact Science Faculty, Northeastern University of Argentina and Institute of Modelling and Innovation on Technology, Corrientes, Argentina

## Correspondence

Gustavo Aucar, Department of Physics, Natural and Exact Science Faculty, Northeastern University of Argentina and Institute of Modelling and Innovation on Technology, IMIT, Corrientes, Argentina. Email: gaa@unne.edu.ar

## Funding information

Consejo Nacional de Investigaciones Científicas y Técnicas, Grant/Award Number: 112-201301-00361; Fondo para la Investigación Científica y Tecnológica, Grant/Award Number: PICT2016-2936; Universidad de Antioquia, Grant/Award Number: Estrategia para la sostenibilidad

## Abstract

An exhaustive exploration using non-relativistic and four-component relativistic formalisms of the potential energy surfaces for the microsolvation of  $\text{Sr}^{2+}$ ,  $\text{Ba}^{2+}$  with up to  $n = 6$  water molecules is presented in this work. A multitude of well defined local minima stabilized by cation  $\cdots$  water and by water  $\cdots$  water interactions are found. Cation  $\cdots$  water contacts transcend the electrostatic interactions of simplistic ionic bonding. The formal charge causes a chaotropic effect in the structure of the solvent affecting water to water hydrogen bonds and inducing water dissociation and microsolvation of the resulting  $\text{H}^+$ ,  $\text{OH}^-$  ions in extreme cases. Relativistic effects are close to 0.7% or smaller in geometries and electronic energies, but they are around 27% for shieldings of  $\text{Ba}^{2+}$  clusters. The nuclei of the central cations are deshielded (around 10% in going from  $n = 1$  to  $n = 3$ ) due to microsolvation.

## KEYWORDS

bonding interactions, microsolvation, nuclear magnetic shieldings, relativistic effects

## 1 | INTRODUCTION

Microsolvation of charged species [1] is a topic with deep implications in areas ranging from atmospheric sciences to molecular biology. A large number of studies have been devoted to the study of systems containing just a few water molecules interacting with cations of both groups I and II in the periodic table [2–14], with heavy emphasis on the lighter, biologically relevant [15–27]  $\text{Na}^+$ ,  $\text{K}^+$ ,  $\text{Mg}^{2+}$ , and  $\text{Ca}^{2+}$ .

Multicharged ions are highly unstable due to Coulomb repulsion, thus, aqueous environments are a common way in nature to provide stabilization. However, the formal charge produces chaotropic/kosmotropic effects on the structure of the solvent [28], heavily influencing the hydrogen bonding networks responsible for the (lack of) structure of liquid water and substantially increasing structural possibilities. In addition, the atomic numbers of Sr (38) and Ba (56) demand the exploration of relativistic effects. The available literature dedicated to the microsolvation of  $\text{Sr}^{2+}$ ,  $\text{Ba}^{2+}$  is mainly focused on the energies and geometries of very limited number of biased structures [4–14], with little to no attention devoted to three very important topics: intensive exploration of structural possibilities, the nature of bonding interactions, and relativistic effects.

The inclusion of relativistic effects in the calculation of electronic properties of heavy-atom containing molecules is mandatory. This is specially the case for molecular properties that are highly dependent on the electron density in the vicinity of nuclei, as happens for nuclear magnetic resonance (NMR) spectroscopic parameters [29, 30]. At the moment, relativistic quantum chemistry is a mature area of research and, so, several and reliable procedures have been developed to include relativistic effects on molecular properties, which are based on four-component,

two-component and one-component Hamiltonians [31–36]. NMR magnetic shieldings have additional constraints regarding the consideration of gauge origin and the way small components are related with large components in four-component procedures [37–39]. Among the different models and theories that have been applied during more than 20 years [40–44], there is the four-component polarization propagator approach, which has the advantage of getting the NR values of the properties straightforwardly making  $c$  (the speed of light in vacuum) go to infinity [45, 46]. Some of us are used to work with those propagators and the unrestricted kinetic balance as a prescription that relates large and small components of the four-component molecular orbitals [47]. although there are several other prescriptions [48, 49].

In previous works [50, 51], it was shown that the radial distribution of the  $H \cdots X$  and  $H-O-H \cdots OH_2$  distances, together with bonding energies are highly affected by relativistic effects in  $[X(H_2O)_n]^-$  ( $X = Br, I, At; n = 1, \dots, 6$ ) clusters. In the case of  $CH_3Hg(H_2O)_n$  ( $n = 1, 2, 3$ ) systems, both, electron correlation and relativistic effects must be included for the accurate calculation of interaction energies. In these last systems relativistic effects cannot be neglected when NMR spectroscopic parameters are studied. In those works as well as here, absolute magnetic shieldings alone and not chemical shifts are considered because these shifts are much less sensitive to relativistic effects.

In this paper we apply stochastic algorithms to exhaustively sample the potential energy surfaces (PESs) for the microsolvation of  $Sr^{2+}$ ,  $Ba^{2+}$  with up to six explicit water molecules, by analyzing bonding interactions using methods firmly rooted in the formalism of quantum mechanics, and by studying relativistic effects using a 4-component methodology [46, 47]. We also offer for the first time in the scientific literature a detailed analysis of the nuclear magnetic shieldings in the central cations due to microsolvation. We have recently published two works concerning the inclusion of relativistic effects on bonding energies and magnetic shieldings during the microsolvation of methylmercury [52] and of heavy halides [51]. In the first case it was found that relativistic effects on the shielding of carbon and oxygen are larger than 10%, but on mercury, those effects are close to 50%! The NMR spectroscopic parameters are also largely influenced by the presence of water molecules. In the case of microsolvation of heavy halides, electron correlation and relativistic effects are of the same order of magnitude though of different sign. Furthermore, relativistic effects on bonding energies are not negligible and depend on whether one includes electron correlation or not. So, another aim of this work is to show how important relativistic and electron correlation effects are on both, binding energies and magnetic shieldings of microsolvated  $Sr^{2+}$  and  $Ba^{2+}$ .

## 2 | COMPUTATIONAL METHODS

The first step in our study is a thorough exploration of the PESs for the  $[M(H_2O)_n]^{2+}$  clusters with  $M = Sr, Ba$ , and  $n = 1 - 6$ . We used ASCEC [53–55], a simulated annealing algorithm with a modified Metropolis acceptance test to generate candidate structures via duplicate runs for each system. Initial assessments of the effect of the level of theory (including various functionals as well as MP2 calculations, see Section 3.1) and of the quality of the basis sets led us to chose PBE0/Def2-TZVPPD as the best compromise between accuracy and computational expense, therefore, all structures afforded by ASCEC were optimized and further characterized as well defined minima via harmonic vibrational analysis using this model chemistry in the Gaussian09 suite of programs [56].

The large set of equilibrium structures obtained with the procedure discussed above were used to analyze the nature of intermolecular water  $\cdots$  water,  $Sr \cdots$  water, and  $Ba \cdots$  water interactions under the Quantum Theory of Atoms in Molecules [57–62] as implemented in the AIMALL program [63]. We derive information about the nature of the interactions from the properties of the associated bond critical points (BCPs,  $r_c$ ) located after analysis of the topology of the corresponding molecular electron density. In particular, we study the following quantities:

1. Accumulation of electron density at the BCP,  $\rho(r_c)$ : larger values are indicative of increasingly covalent interactions, while smaller values are indicative of either weak, long distance contacts, or of ionic interactions
2. Energy densities: The kinetic energy density,  $\mathcal{G}(r_c)/\rho(r_c)$ , is always positive and repulsive. The potential energy density,  $\mathcal{V}(r_c)/\rho(r_c)$ , is always negative and attractive. Therefore, the sign of the total energy density  $\mathcal{H}(r_c)/\rho(r_c) = \mathcal{G}(r_c)/\rho(r_c) + \mathcal{V}(r_c)/\rho(r_c)$  determines whether electrons are attracted or repelled from the BCP, thus, positive local total energy densities are indicative of interactions for which the electron density is pushed away from the BCP toward the nuclei, describing weak, long range or ionic bonds, while negative local total energy densities indicate favorable conditions for local concentration of electron charge, proper of covalent bonds. An alternative dimensional analysis leads to the same conclusions: energy density has the same units as pressure, therefore, local total energy densities are equated to local quantum pressures exerted on the electrons at the BCPs [61], thus, positive pressures push electrons away (weak and long range interactions) while negative pressure regions are strong electron attractors (covalent interactions)
3. Virial ratio: Local application of the virial theorem at BCPs lead Espinosa and coworkers [64] to establish the following classification for the nature of bonding interactions:

$$\frac{|\mathcal{V}(r_c)|}{\mathcal{G}(r_c)} = \begin{cases} \leq 1 & \text{Long range, ionic, hydrogen bonds} \\ \in [1, 2] & \text{Intermediate character} \\ \geq 2 & \text{Covalent bonding} \end{cases} \quad (1)$$

Binding energies for each isomer,  $BE_i^{MW_n}$ , were computed as the difference between the energy of the fragments  $E_j$  and the energy of the particular cluster,  $E_i^{MW_n}$ :

$$BE_i^{MW_n} = \sum_j^{\text{fragments}} E_j - E_i^{MW_n} \quad (2)$$

in this way, positive binding energies indicate that the cluster is stabilized with respect to the isolated water molecules and cation. For the systems studied here, experimental sequential hydration enthalpies and sequential hydration Gibbs free energies are available [65, 66] for clusters containing both  $Ba^{2+}$  and  $Sr^{2+}$ . Consequently, not only as means of validating our methods, but also as a predictive tool to characterize the new structures located in this work, we calculated both quantities according to the following procedure using harmonic vibrations whenever needed: first we considered the sequential hydration reactions



the hydration energy  $\Delta E^{MW_n}$  (enthalpy or Gibbs) here is

$$\Delta E^{MW_n} = E^{MW_n} - (E^W + E^{MW_{n-1}}) \quad (4)$$

In Equation (4),  $E^W$  is the energy of an isolated water molecule in its equilibrium geometry,  $E^{MW_{n-1}}$  represents the hydration energy for the system with  $n - 1$  water molecules, with  $E^{MW_n}$  calculated as

$$E^{MW_n} = \sum_i x_i E_i^{MW_n} \quad (5)$$

where  $x_i$  is the concentration of isomer  $i$  within hypothetical pure samples of  $[M(H_2O)_n]^{2+}$  clusters, estimated at room conditions (298.15 K, 1 bar) using a Boltzmann distribution of the energies:

$$x_i = \frac{e^{-E_i^{MW_n}/k_B T}}{\sum_i e^{-E_i^{MW_n}/k_B T}} \quad (6)$$

Strontium and barium are located in periods 5, 6 of the periodic table, thus, it is expected that relativistic effects would be at least of the same order of magnitude as those known to occur in silver and gold, which belong to the same periods. The dications are expected to magnify those effects because the remaining electrons are more tightly bound to the nucleus. 4-component (4c) relativistic formalism is considerably more complex than standard non-relativistic (NR) formulations of electronic structure methods, and thus are orders of magnitude more expensive to calculate. Accordingly, to assess relativistic effects in the microsolvation of  $Sr^{2+}$ ,  $Ba^{2+}$ , we devised the following strategy, limiting ourselves to no more than three water molecules (all calculations were carried out using the DIRAC code [67]):

1. We took the global minimum from the  $n = 1, 2$  surfaces and fully optimized them using 4c Dirac-Hartree-Fock (4c-DHF) and PBE0 (4c-PBE0) levels in conjunction with the dyall.ae2z, dyall.v3z, dyall.cv3z, dyall.ae3z, dyall.v4z, dyall.cv4z, dyall.ae4z basis sets [68]. This allows us to analyze the convergence as the size of the basis set increases, besides including electron correlation within a relativistic framework
2. As shown in section 6 of the Supporting Information, because of the very small variations at a reasonable computational cost when compared against the very accurate and expensive dyall.ae4z basis set, we selected the dyall.cv4z basis set to optimize the global minimum for  $n = 3$  at the same 4c-DHF and 4c-PBE0 levels
3. Nuclear magnetic shieldings on all atoms,  $\sigma(Ba), \sigma(Sr), \sigma(O), \sigma(H)$ , were calculated on all relativistic 4c-DHF and 4c-PBE0 geometries using the polarization propagator method [46] under the random phase approximation (RPA) with unrestricted kinetic balance conditions (UKB) [69] as implemented in DIRAC [67]. London atomic orbitals (LAO) were used in order to obtain the independence of the property with the gauge origin. The use of LAO together with the UKB prescription is equivalent to the magnetic balance prescription [47]. The dyall.cv4z basis set was also used for this purpose
4. Relativistic effects are calculated comparing 4c results against non-relativistic values, which, in order to use the same scheme of calculation, are obtained after scaling the speed of light to  $c = 100c_0$ , where  $c_0$  is the speed of light in vacuum. This procedure was used in early works where we showed that this scheme of calculation converges to non-relativistic values [46, 69, 70]. The scheme selected here for the relativistic

calculations and for obtaining relativistic effects follows procedures previously developed in our group [69]. Electron correlation effects may be different when obtained within a relativistic framework or within a non-relativistic framework. Then, scaling the speed of light to a large enough value ensures that both calculations are performed with the same code and theoretical model.

### 3 | RESULTS AND DISCUSSION

#### 3.1 | Selection of the model chemistry

MP2 and DFT methods are among the most popular choice in previous reports on the microsolvation of group II dications [5–8, 11, 12, 71]. Accordingly, we chose MP2, B3LYP, M06-2X, PBE0 in conjunction with SDDALL, 6-311++G\*\*, Def2-TZVP, and Def2-TZVPPD basis sets and the corresponding pseudopotentials of heavy atoms to test the reproducibility of the experimental hydration enthalpies and hydration free energies for  $[\text{Sr}(\text{H}_2\text{O})_2]^{2+}$  and  $[\text{Ba}(\text{H}_2\text{O})_2]^{2+}$ , the results are listed in Table 1. Notice that the thermodynamic quantities reported in Table 1 include contributions from all clusters for  $n=2$  (see Figure 1) and thus all ion-ligand and hydrogen bond interactions are properly accounted for in the process of selecting an adequate computational model. It is quite remarkable that for the particular problem at hand, DFT methods consistently afford better hydration enthalpies and free energies than second order perturbation theory. It is also seen that the thermodynamic quantities are a bit sensitive to the choice of basis set, with errors generally not exceeding 5% with an extreme case of 6.9% error with respect to the experimental sequential hydration enthalpy for  $[\text{Ba}(\text{H}_2\text{O})_2]^{2+}$  at the PBE0/6-311++G\*\* level. For the remaining of this work we chose to study all molecular clusters using the PBE0/Def2-TZVPPD model chemistry because of the excellent results shown in Table 1 (errors not exceeding 3%) and because this particular functional has proven very accurate in the calculation of relativistic magnetic resonance parameters [72], which we will discuss below.

#### 3.2 | Structural issues

Our stochastic sampling of the PESs of the title clusters uncovered a rich structural diversity previously unnoticed in the literature. Figure 1 shows all 46 geometrical motifs found in this work, spread by cluster composition as 1, 2, 5, 7, 14, 17 motifs for  $n=1-6$  respectively. A geometrical motif is defined [73–75] as the connectivity between fragments, that is, as the spatial disposition dictated by the  $\text{M}\cdots\text{O}$  contacts and by the hydrogen bonds in a particular cluster, consequently, a particular motif may have several different isomers because of the relative positions of

**TABLE 1** Hydration enthalpies ( $\Delta H$ ) and hydration free energies ( $\Delta G$ ) at room conditions for  $[\text{Sr}(\text{H}_2\text{O})_2]^{2+}$  and  $[\text{Ba}(\text{H}_2\text{O})_2]^{2+}$  calculated at several levels of theory

Method	$[\text{Sr}(\text{H}_2\text{O})_2]^{2+}$		$[\text{Ba}(\text{H}_2\text{O})_2]^{2+}$	
	$\Delta H$	$\Delta G$	$\Delta H$	$\Delta G$
MP2/SDDALL/6-311++G**	−38.5	−31.8	−32.5	−24.4
MP2/Def2-TZPD	−39.3	−31.4	−32.6	−25.0
MP2/Def2-TZVPPD	−36.2	−30.7	−29.6	−24.6
B3LYP/SDDALL/6-311++G**	−41.7	−35.6	−36.3	−28.5
B3LYP/Def2-TZPD	−42.0	−36.4	−35.8	−29.5
B3LYP/Def2-TZVPPD	−40.7	−32.4	−34.2	−27.5
M06-2X/SDDALL/6-311++G**	−43.1	−34.6	−37.5	−29.7
M06-2X/Def2-TZPD	−42.9	−34.9	−37.1	−28.7
M06-2X/Def2-TZVPPD	−41.5	−33.5	−35.9	−28.3
PBE0/SDDALL/6-311++G**	−42.3	−35.9	−37.2	−29.3
PBE0/Def2-TZPD	−42.4	−35.8	−36.4	−29.7
PBE0/Def2-TZVPPD	−40.7	−34.9	−35.0	−28.7
Experimental [65, 66]	−41.37 (1.12)	−35.92 (1.15)	−34.80 (1.55)	−28.51 (1.67)

Note: All energies in kcal/mol. Experimental values are also included. The SDDALL/6-311++G\*\* combination means that SDDALL pseudopotentials were used for Sr, Ba, and that the 6-311++G\*\* basis set was used for O, H.

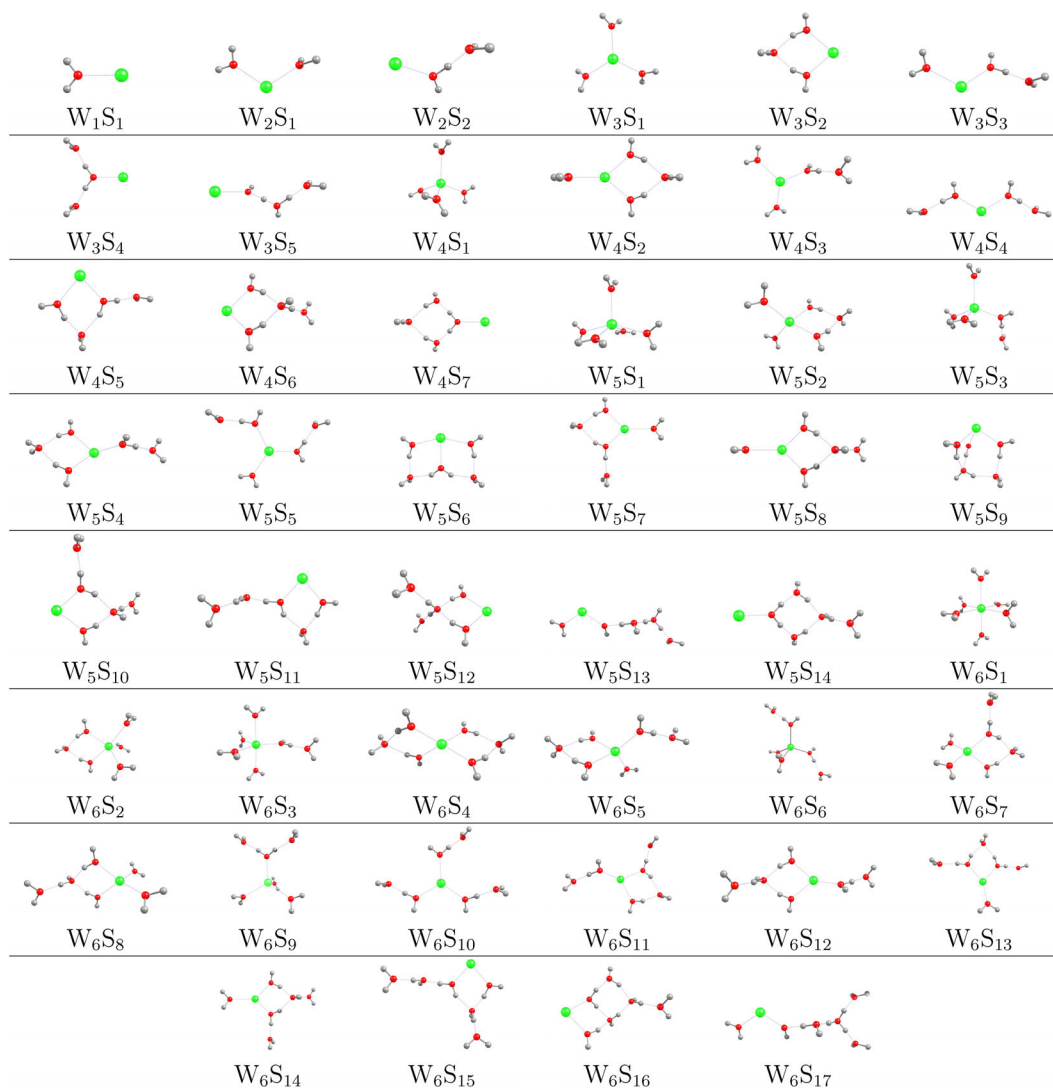


**FIGURE 1** Structural motifs on the PBE0/Def2-TZVPPD potential energy surfaces for the  $[M(H_2O)_n]^{2+}$  clusters,  $M = Sr, Ba$ ,  $n = 1 - 6$ . In  $W_3S_5$  and in  $W_5S_{13}$ , charge induced water dissociation and diffusion of the liberated proton are seen. See Table 3 for relative energies and for classification into Sr, Ba clusters. All structures are common to both cations, except  $W_6S_9$ , which is not present for Sr. The  $W_nS_m$  notation indicates that in the energy scale,  $W_6S_5$  is the fifth lowest energy structure for all clusters containing six water molecules

the hydrogen atoms not taking part in the hydrogen bonding network, thus the total number of equilibrium structures is considerably larger than the bare number of motifs.

Remarkably, a few high energy structures ( $W_3S_5$ ,  $W_5S_{13}$  in Figure 1) show that for both cations, the perturbative effect of the formal charge is so strong that it induces water dissociation and subsequent solvation of the  $OH^- + H^+$  pair. Evidence of water dissociation is not only gathered after mere visual inspection of the molecular geometries in Figure 1, indeed, a quantitative relationship between symmetry ( $q_1$ ) and size ( $q_2$ ) for hydrogen bonds is provided in the form of a Stern–Limbach plot [76] in Figure 2. This plot reveals a very complex picture of the nature of hydrogen bonds that seems independent of the identity of the central cation: large negative values of  $q_1$  (the far upper left region of the quadratic trend) indicate long hydrogen bonds and very weak intermolecular interactions while smaller negative values near the minimum indicate shorter, stronger interactions. The region of positive  $q_1$  indicates proton transfer, thus the gap between positive and negative values indicates that the  $O-H\cdots O$  pair of interactions can only be stretched to a certain degree before the proton is transferred to form  $O\cdots H-O$ . The fact that  $q_1$  covers a wide range of distances indicates that all sorts of hydrogen bonds are present in the microsolvation of divalent cations, from the classical  $O-H\cdots O-H$  picture to the partially transferred  $O\cdots H\cdots O-H$  cases in which the hydrogen atom at the center of the HB cannot be assigned to any of the oxygen atoms. Furthermore, since our starting molecular geometries only considered well defined water molecules,  $W_5S_{13}$  suggests that once water molecules in direct contact with the cation have been dissociated, the proton has diffused its way to at least the third, possibly even the fourth solvation shell in a way reminiscent of the Grotthus mechanism [77]  $M\cdots OH\cdots OH\cdots OH\cdots OH_2 \rightarrow M\cdots(O-H)\cdots H_2O\cdots(H_3O)^+\cdots OH_2$ .

Figure 3 shows radial distribution functions for all  $M\cdots O$ ,  $H-O\cdots H$  interactions as well as for all  $O-H$  distances resulting after proton abstraction. After inclusion of  $Mg\cdots O$ ,  $Ca\cdots O$  from the literature [2],  $M\cdots O$  distances correlate with the number of electrons surrounding the

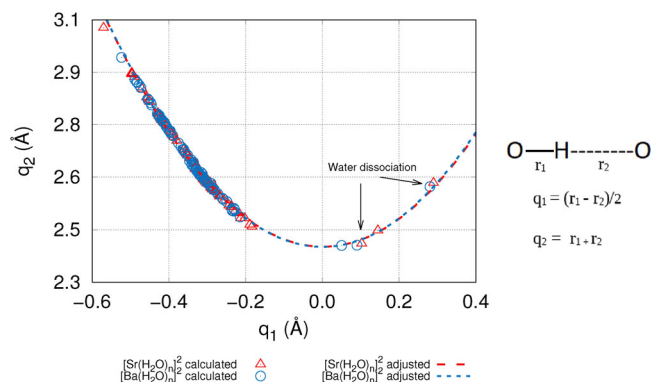


**FIGURE 2** Correlation between symmetry ( $q_1$ ) and size ( $q_2$ ) for the O—H···O distances in the microsolvation of  $\text{Sr}^{2+}$ ,  $\text{Ba}^{2+}$  with up to six water molecules

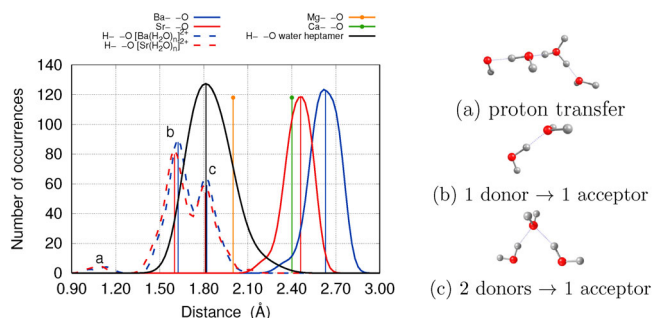


**FIGURE 3** Radial distribution functions obtained using a standard kernel density estimation [78] for the discrete set of O—H···O distances in hydrogen bonds and for metal···O interactions in the microsolvation of  $\text{Sr}^{2+}$ ,  $\text{Ba}^{2+}$ , taken from the PBE0/Def2-TZVPPD optimized geometries. The corresponding Mg···O, Ca···O distances were reported by Gonzalez and coworkers [2] and are included here for comparison

**TABLE 2** Sequential hydration enthalpies and Gibbs free energies at the PBE0/Def2-TZVPPD level for the microsolvation of  $\text{Ba}^{2+}$ ,  $\text{Sr}^{2+}$  at room conditions calculated using the procedure described in Equations (3)–(6)

n	$\Delta H$ (kcal/mol)				$\Delta G$ (kcal/mol)			
	$[\text{Sr}(\text{H}_2\text{O})_n]^{2+}$		$[\text{Ba}(\text{H}_2\text{O})_n]^{2+}$		$[\text{Sr}(\text{H}_2\text{O})_n]^{2+}$		$[\text{Ba}(\text{H}_2\text{O})_n]^{2+}$	
	This work	Experimental	This work	Experimental	This work	Experimental	This work	Experimental
1	−46.2	−49.14 (1.46)	−39.6	−41.25 (1.15)	−41.3	−42.33 (1.46)	−34.9	−34.63 (1.15)
2	−40.7	−41.37 (1.12)	−35.0	−34.80 (1.55)	−34.9	−35.92 (1.15)	−28.7	−28.51 (1.67)
3	−35.9	−34.82 (1.22)	−30.8	−30.88 (0.93)	−28.1	−26.15 (1.24)	−23.4	−23.23 (0.93)
4	−31.6	−29.92 (0.86)	−27.3	−25.69 (0.96)	−23.4	−22.01 (0.93)	−19.8	−19.41 (1.15)
5	−25.5	−24.95 (0.84)	−22.2	−22.16 (1.50)	−15.7	−15.03 (0.88)	−15.2	−13.05 (1.53)
6	−22.7	−22.63 (0.64)	−20.2	−18.50 (1.29)	−14.6	−13.02 (0.72)	−12.2	−10.13 (1.39)

Note: Experimental values [65, 66] (with uncertainties) are provided for comparison.

cation, thus,  $d_{\text{Mg}\cdots\text{O}} < d_{\text{Ca}\cdots\text{O}} < d_{\text{Sr}\cdots\text{O}} < d_{\text{Ba}\cdots\text{O}}$ . The distribution of O···H distances is quite interesting. First, we have the very small peaks centered around 1 Å for both cations, signaling proton transfer. There are two peaks in the radial distribution of hydrogen bonds, this charge induced splitting of the radial distribution is clear evidence that not all hydrogen bonds are equal as shown in the (a)–(c) insets. The tallest peak, centered at  $\approx 1.60$  Å for Sr and at  $\approx 1.63$  Å for Ba indicates a sensible strengthening of the hydrogen bonds when compared to the bare water clusters.

### 3.3 | Energies

Table 2 lists the expected values, calculated as statistical averages over all clusters at a given size (Equations 5 and 6), for the sequential hydration enthalpies and Gibbs free energies at room conditions for  $\text{Sr}^{2+}$ ,  $\text{Ba}^{2+}$ . The first clear observation is that our model chemistry accurately

reproduces experimental values, thus providing strong support to our methods. Indeed, most errors are below 5% and well within experimental uncertainty.

Table 3 lists all binding energies computed using Equation (2) and relative energies within each PES. All clusters are strongly bound. The electrophilic power of a cation,  $\epsilon_{M^{q+}}$ , is a measure of the electron-seeking ability of the cation [79]. Because of the size of the cation, and because of the number of electrons surrounding the nucleus, the electrophilic power of alkaline earth metals is a property that decreases going down in the periodic table of the elements, that is,  $\epsilon_{Mg^{2+}} > \epsilon_{Ca^{2+}} > \epsilon_{Sr^{2+}} > \epsilon_{Ba^{2+}}$ . This trend is recovered with the corresponding ranges of binding energies: according to Gonzalez and coworkers [2], and according to Table 3, up to 314, 241, 201, 175 kcal/mol are obtained for the microsolvation of  $Mg^{2+}$ ,  $Ca^{2+}$ ,  $Sr^{2+}$ ,  $Ba^{2+}$ , respectively. It is worth noticing that for the doubly charged cations, from a purely energetic point of view, a maximum coordination of the central cation with water molecules is preferred up to  $n = 6$ , however, for smaller cations with fewer electrons ( $Li^+$ , e.g., Romero et al. [3]), the electrophilic power is such that even when five or more water molecules are available for microsolvation, a maximum coordination of  $n = 4$  is preferred, the excess solvent molecules attaching to the  $[Li(H_2O)_4]^+$  cluster via hydrogen bonds in a second solvation shell. Furthermore, weakly bonded clusters are extremely difficult to analyze because their PESs are populated by large numbers of local minima very close in energy, thus, many structures contribute to experimental signals, conversely, in the explicit microsolvation of  $Sr^{2+}$ ,  $Ba^{2+}$  with up to six water molecules, the electrophilic power of the cations is such that a dominant minimum, corresponding to the maximum coordination of the central cation, with Gibbs free energy based populations exceeding 99% is always observed, regardless of the number of water molecules.

The data in Table 3 is quite descriptive of the microsolvation process, but is far removed from bulk properties, that is, as  $n$  grows, the strength of the overall interactions increases, with larger binding energies for  $Sr^{2+}$  at all cluster compositions, however, the expected asymptotic trend for large  $n$  for both cations is clearly not attained up to  $n = 6$ .

### 3.4 | Dissection of bonding interactions

We use the tools provided by the Quantum Theory of Atoms In Molecules (QTAIM [57–62]) as well established tools to analyze bonding interactions. Figure 4 shows the accumulation of electron density at BCPs for all types of intermolecular interactions, arising because of the microsolvation of  $Sr^{2+}$ ,  $Ba^{2+}$ , as a function of fragment separation. Figure 5 shows the corresponding virial ratios. A few stern conclusions may be drawn from those plots:

1. There are highly correlated exponential decays of the electron densities at BCPs as the fragment separation increases, regardless of the type of the interaction ( $M \cdots O$ ,  $O-H \cdots O$ ) and regardless of the identity of the cation. This generalized exponential decay [73, 79–82] is physically meaningful because it correctly describes the asymptotic  $\rho(r_c) \rightarrow 0$  as  $r \rightarrow \infty$  behavior.
2. All  $Sr \cdots O$  interactions fall within the same adjusted line, which is different to the adjusted line for the  $Ba \cdots O$  interactions. Moreover, all  $O \cdots H$  interactions, either hydrogen bonds or formal  $O-H$  bonds, regardless of their environment, belong to the same line. Therefore, in a very formal, general sense, the accumulation of electron density at the corresponding BCP suffices to characterize each type of binary interaction [82, 83].
3. Even the highly ionic  $Sr \cdots O$ ,  $Ba \cdots O$  contacts have non-negligible degrees of accumulation of electron density in the intermediate region between the atoms, at the corresponding BCP, thus, very much in the lines of the original works of Pauling [84] and Coulson [85], ionic bonding does not arise from a simplistic separation of charges.
4. Additional support for the complex nature of  $M \cdots O$  interactions is obtained from the virial ratios at BCPs:  $M \cdots O$  contacts are characterized as either long range ( $\mathcal{V}(r_c)/\mathcal{G}(r_c) < 1$ , mostly ionic in this case) or as of intermediate character ( $1 < \mathcal{V}(r_c)/\mathcal{G}(r_c) < 2$ , with contributions from ionic and covalent interactions).
5. The vast majority of hydrogen bonds fall in the intermediate category, with just a couple of long range cases. This is also a manifestation of the strong chaotropic effect that the formal charge has on the molecular structure of the solvent [1, 79], since the hydrogen bond in the isolated water dimer is well characterized as strictly long range.

### 3.5 | Relativistic and correlation effects

Comparing the results shown in Tables 3 and 4 it is seen that bonding energies depend on whether they are calculated with pseudopotentials or with 4c methods. These last, and most accurate methods, give larger bonding energies whose relativistic contributions increase with the number of water molecules. For Ba such differences are 5.0%, 5.6% and 5.7% for  $W_1S_1$ ,  $W_2S_1$  and  $W_3S_1$  respectively.

In order to devise a robust computational method to assess relativistic and correlation effects it is necessary to select a basis set that properly balances accuracy and computational cost. Thus, we took  $W_1S_1$  and  $W_2S_1$ , the global minima for  $n = 1, 2$  in the PES for the microsolvation of each



**TABLE 3** Structural and energetic parameters for the microsolvation of Sr<sup>2+</sup>, Ba<sup>2+</sup>

Motif	Heavy-atom symmetry	<i>m</i>	HB	$\Delta E_B$		Relative $\Delta E_B$	
				$[\text{Sr}(\text{H}_2\text{O})_n]^{2+}$	$[\text{Ba}(\text{H}_2\text{O})_n]^{2+}$	$[\text{Sr}(\text{H}_2\text{O})_n]^{2+}$	$[\text{Ba}(\text{H}_2\text{O})_n]^{2+}$
W <sub>1</sub> S <sub>1</sub>	C <sub>2v</sub>	1	0	46.7	40.2	0.0	0.0
W <sub>2</sub> S <sub>1</sub>	C <sub>2v</sub>	2	0	87.2	75.0	0.0	0.0
W <sub>2</sub> S <sub>2</sub>	C <sub>s</sub>	1	1	74.2	65.5	13.0	9.4
W <sub>3</sub> S <sub>1</sub>	C <sub>3</sub>	3	0	122.8	105.6	0.0	0.0
W <sub>3</sub> S <sub>2</sub>	C <sub>2v</sub>	2	2	111.8	98.2	11.1	7.4
W <sub>3</sub> S <sub>3</sub>	C <sub>1</sub>	2	1	111.5	97.6	11.3	8.1
W <sub>3</sub> S <sub>4</sub>	C <sub>2v</sub>	1	2	95.9	86.2	26.9	19.5
W <sub>3</sub> S <sub>5</sub>	C <sub>1</sub>	1	2	95.0	85.3	27.8	20.3
W <sub>4</sub> S <sub>1</sub>	T <sub>d</sub>	4	0	154.2	132.9	0.0	0.0
W <sub>4</sub> S <sub>2</sub>	C <sub>s</sub>	3	2	145.2	126.9	9.0	6.0
W <sub>4</sub> S <sub>3</sub>	C <sub>1</sub>	3	1	144.6	126.9	9.6	7.0
W <sub>4</sub> S <sub>4</sub>	C <sub>2v</sub>	2	2	134.2	118.7	20.0	14.2
W <sub>4</sub> S <sub>5</sub>	C <sub>s</sub>	2	3	133.2	118.2	21.0	14.7
W <sub>4</sub> S <sub>6</sub>	C <sub>s</sub>	2	3	131.0	116.6	23.2	16.3
W <sub>4</sub> S <sub>7</sub>	C <sub>s</sub>	1	4	110.6	100.3	44.6	32.6
W <sub>5</sub> S <sub>1</sub>	C <sub>2v</sub>	5	0	179.2	155.0	0.0	0.0
W <sub>5</sub> S <sub>2</sub>	C <sub>2v</sub>	4	2	175.1	152.5	4.2	2.5
W <sub>5</sub> S <sub>3</sub>	C <sub>1</sub>	4	1	173.9	151.3	5.4	3.8
W <sub>5</sub> S <sub>4</sub>	C <sub>1</sub>	3	3	165.8	146.1	13.5	8.9
W <sub>5</sub> S <sub>5</sub>	C <sub>1</sub>	3	2	165.0	145.0	14.3	10.1
W <sub>5</sub> S <sub>6</sub>	C <sub>s</sub>	3	4	164.5	145.4	14.7	9.6
W <sub>5</sub> S <sub>7</sub>	C <sub>1</sub>	3	3	164.4	144.9	14.8	10.1
W <sub>5</sub> S <sub>8</sub>	C <sub>s</sub>	3	3	163.1	144.0	16.1	11.0
W <sub>5</sub> S <sub>9</sub>	C <sub>s</sub>	3	4	161.6	142.9	17.6	12.8
W <sub>5</sub> S <sub>10</sub>	C <sub>1</sub>	2	4	150.4	134.8	28.8	20.2
W <sub>5</sub> S <sub>11</sub>	C <sub>1</sub>	2	4	148.9	133.2	30.3	21.9
W <sub>5</sub> S <sub>12</sub>	C <sub>2v</sub>	2	4	147.5	132.4	31.8	22.7
W <sub>5</sub> S <sub>13</sub>	C <sub>1</sub>	2	3	144.5	128.5	34.8	26.5
W <sub>5</sub> S <sub>14</sub>	C <sub>s</sub>	1	5	124.8	114.3	54.4	40.8
W <sub>6</sub> S <sub>1</sub>	O <sub>h</sub>	6	0	201.8	175.1	0.0	0.0
W <sub>6</sub> S <sub>2</sub>	C <sub>1</sub>	5	2	199.1	173.9	2.7	1.2
W <sub>6</sub> S <sub>3</sub>	C <sub>s</sub>	5	1	197.0	172.1	4.8	3.0
W <sub>6</sub> S <sub>4</sub>	D <sub>2d</sub>	4	4	194.9	171.1	7.0	4.0
W <sub>6</sub> S <sub>5</sub>	C <sub>s</sub>	4	3	193.7	170.1	8.2	5.0
W <sub>6</sub> S <sub>6</sub>	C <sub>2</sub>	4	2	192.4	168.7	9.4	6.4
W <sub>6</sub> S <sub>7</sub>	C <sub>s</sub>	4	3	192.4	168.9	9.4	6.2
W <sub>6</sub> S <sub>8</sub>	C <sub>s</sub>	4	3	191.7	168.6	10.1	6.5
W <sub>6</sub> S <sub>9</sub>	C <sub>s</sub>	4	2	-	166.5	-	8.6
W <sub>6</sub> S <sub>10</sub>	C <sub>1</sub>	3	3	184.0	162.6	17.8	12.4
W <sub>6</sub> S <sub>11</sub>	C <sub>1</sub>	3	4	183.8	163.0	18.0	12.1
W <sub>6</sub> S <sub>12</sub>	C <sub>s</sub>	3	4	182.8	162.4	19.0	12.7
W <sub>6</sub> S <sub>13</sub>	C <sub>s</sub>	3	4	182.2	161.6	19.6	13.5
W <sub>6</sub> S <sub>14</sub>	C <sub>1</sub>	3	4	180.6	160.5	21.3	14.6
W <sub>6</sub> S <sub>15</sub>	C <sub>1</sub>	2	5	164.9	148.7	36.9	26.4
W <sub>6</sub> S <sub>16</sub>	C <sub>1</sub>	2	6	160.6	145.0	41.3	30.1
W <sub>6</sub> S <sub>17</sub>	C <sub>1</sub>	2	4	160.8	144.6	41.1	30.5

Note: *m* is the coordination number of the metal atom; HB is the number of hydrogen bonds within the cluster.  $\Delta E_B$  is the binding energy estimated via Equation (2). Relative binding energies with respect to the global minimum on each PES. All data from the PBE0/Def2-TZVPPD optimized geometries.



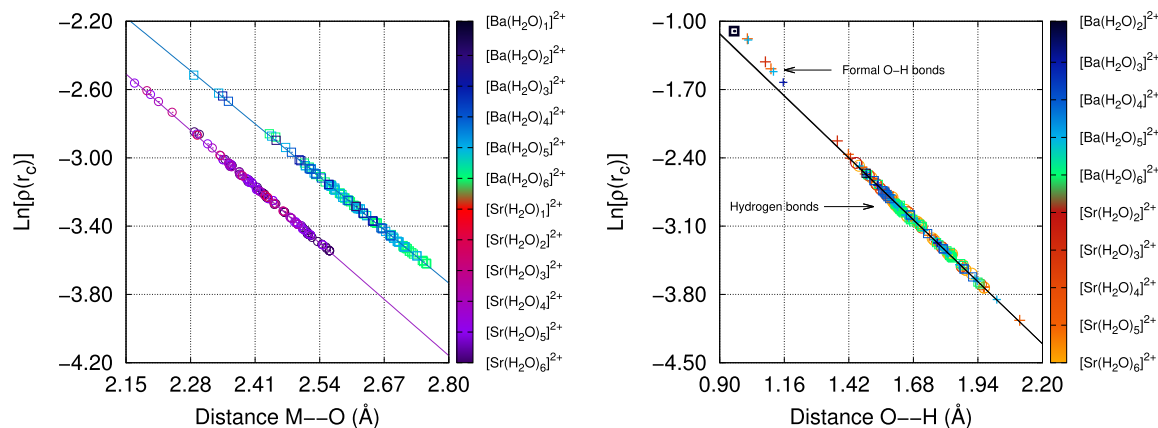


**FIGURE 4** Exponential decays of the electron densities at bond critical points,  $\rho(r_c)$ , for the  $M \cdots O$  (left) and for the  $O \cdots H$  interactions (right) as a function of interaction distance. The isolated water molecule is included for comparison. Purple fit ( $Sr \cdots O$ ):  $\ln[\rho(r_c)] = 2.94 - 2.54d$ ,  $R^2 = .998$ . Blue fit ( $Sr \cdots O$ ):  $\ln[\rho(r_c)] = 2.96 - 2.39d$ ,  $R^2 = .998$ . Black fit ( $O \cdots H$ ):  $\ln[\rho(r_c)] = 1.08 - 2.45d$ ,  $R^2 = .992$

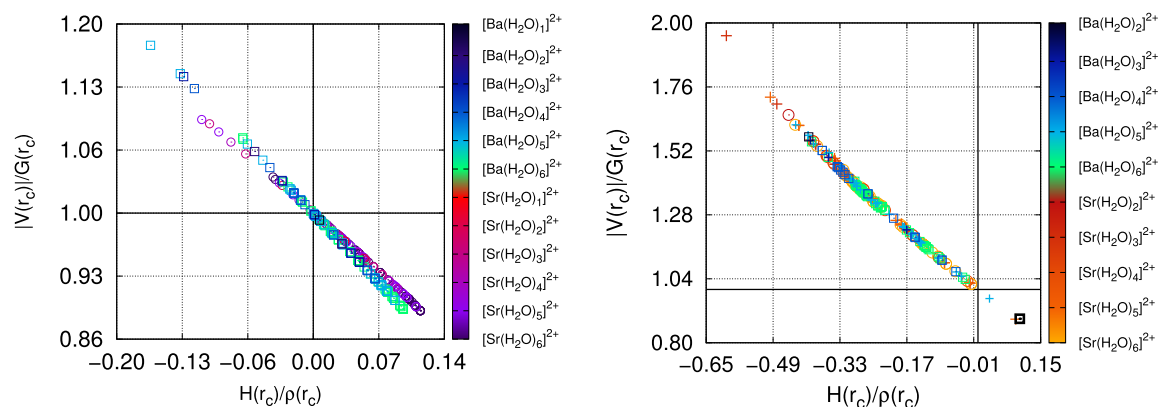


**FIGURE 5** Virial ratios  $|V|/G$  as a function of the bond degree parameter  $\mathcal{H}/\rho$  computed at the bond critical points for the  $M \cdots O$  (left) and  $O \cdots H$  (right) interactions in the PBE0/Def2-TZVPPD optimized geometries. The isolated water dimer is included for comparison

**TABLE 4** Relativistic and correlation (up to PBE0) effects on the purely electronic binding energies (kcal/mol) for the global minima in the  $[M(H_2O)_n]^{2+}$  clusters ( $M = Sr, Ba, n = 1, 2, 3$ )

n	DHF			PBE0			CE (NR) (%)	CE (4c) (%)
	NR	4c	RE (%)	NR	4c	RE (%)		
$[Sr(H_2O)_n]^{2+}$								
1	45.5	45.8	0.7	49.3	49.4	0.2	8.4	7.9
2	85.8	86.3	0.6	92.0	92.4	0.4	7.2	7.1
3	121.9	122.7	0.7	129.7	130.3	0.5	6.4	6.2
$[Ba(H_2O)_n]^{2+}$								
1	37.9	38.4	1.3	42.3	42.4	0.2	11.6	10.4
2	71.7	72.6	1.3	79.0	79.2	0.3	10.2	9.1
3	102.0	103.4	1.4	111.3	112.0	0.6	9.1	8.3

Note: Non-relativistic values are obtained by scaling the speed of light  $c = 100c_0$  ( $c$  the speed of light in vacuum). %RE and %CE correspond to relativistic and correlation effects respectively.

cation and studied the influence of several basis sets in geometrical parameters and binding energies in both regimes, NR and 4c. As seen in section 1 of the Supporting Information, the choice of basis set has little influence on the geometries but has an important influence on binding energies and nuclear magnetic shieldings. Thus, we chose the dyall.c4vz basis set for all further calculations.

**TABLE 5** Relativistic and correlation (up to PBE0) effects on M···O distances (Å) for the global minima in the  $[M(H_2O)_n]^{2+}$  clusters (M = Sr, Ba,  $n = 1, 2, 3$ )

n	DHF			PBE0			CE (NR) (%)	CE (4c) (%)
	NR	4c	RE (%)	NR	4c	RE (%)		
$[Sr(H_2O)_n]^{+2}$								
1	2.45	2.44	0.4	2.38	2.38	0.0	2.9	2.5
2	2.48	2.48	0.0	2.43	2.42	0.4	2.0	2.4
3	2.52	2.51	0.4	2.46	2.46	0.0	2.4	2.0
$[Ba(H_2O)_n]^{+2}$								
1	2.65	2.64	0.4	2.56	2.55	0.4	3.4	3.4
2	2.69	2.68	0.4	2.60	2.59	0.4	3.3	3.4
3	2.73	2.71	0.7	2.64	2.63	0.4	3.3	3.0

Note: Non-relativistic values are obtained by scaling the speed of light to  $c = 100c_0$  ( $c_0$  the speed of light in vacuum). %RE and %CE correspond to relativistic and correlation effects respectively.

**TABLE 6** Nuclear magnetic shieldings  $\sigma(M)$  for the microsolvation of  $Ba^{2+}$ ,  $Sr^{2+}$  with up to three explicit water molecules ( $n = 0$ : Isolated ion)

n	DHF			PBE0			CE (NR) (%)	CE (4c) (%)
	NR	4c	RE (%)	NR	4c	RE (%)		
$[Sr(H_2O)_n]^{+2}$								
0	3480.24	3880.93	11.5	3480.23	3888.83	11.7	0.0	0.2
1	3389.87	3794.84	11.9	3356.14	3762.19	12.1	1.0	0.9
2	3305.94	3706.73	12.1	3247.52	3649.45	12.4	1.8	1.5
3	3057.46	3449.80	12.8	3032.57	3551.62	17.1	0.8	3.0
$[Ba(H_2O)_n]^{+2}$								
0	5911.11	7489.55	26.7	5911.46	7472.40	26.4	0.0	0.2
1	5793.21	7348.51	26.8	5739.90	7298.52	27.2	0.9	0.7
2	5681.25	7222.84	27.1	5590.25	7136.27	27.7	1.6	1.2
3	5577.33	7108.64	27.5	5457.99	6992.21	28.1	2.1	1.6

Note: All calculations were performed using the dyall.cv4z basis set. The percentages of relativistic (RE) and correlation (CE) effects (up to PBE0) are provided.

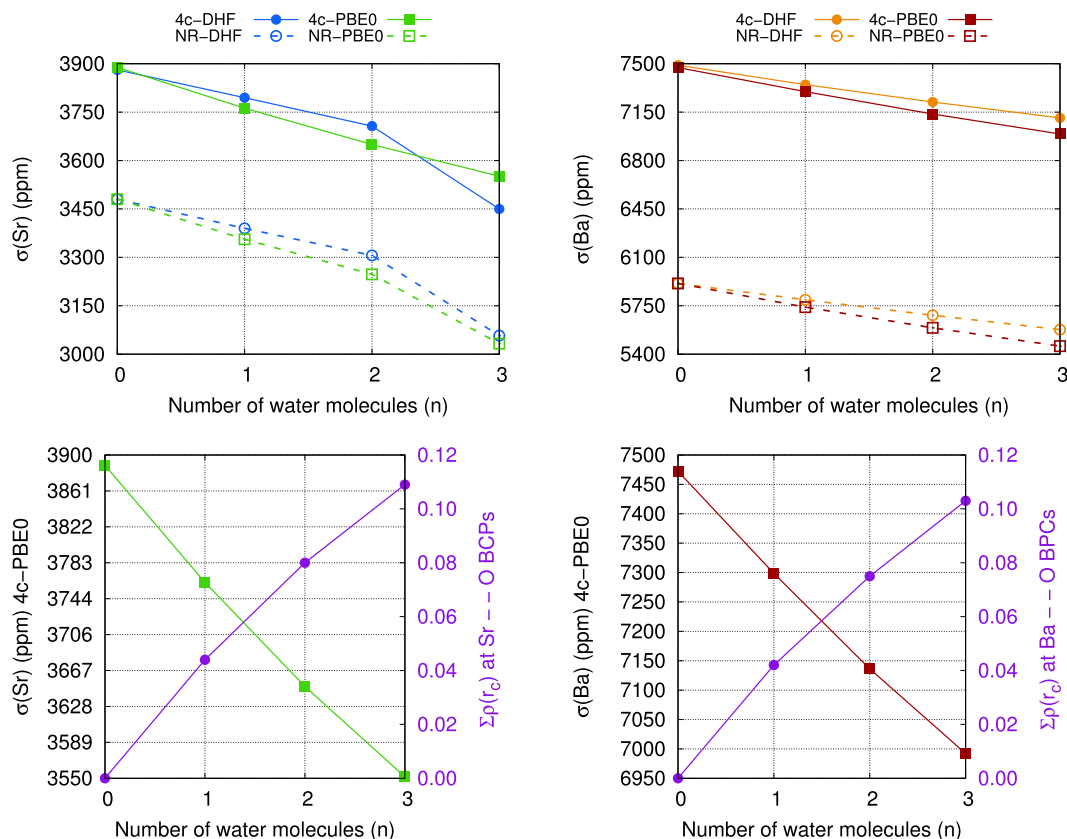
### 3.5.1 | Structures and energies

Table 5 lists M···O distances for the global minima in the  $[M(H_2O)_n]^{2+}$  clusters, M = Sr, Ba,  $n = 1, 2, 3$ , resulting after 4c and NR geometry optimization, at DHF and PBE0 levels. Table 4 lists the corresponding binding energies.

At each level of theory (4c-DHF, 4c-PBE0, and NR) the same geometrical motifs are found in all cases, that is, only small variations in bond lengths are observed without changes in connectivity. Relativistic effects in M···O bond distances do not exceed 0.7% for Ba clusters at the 4c-DHF level, while correlation effects are somewhat larger, going up to 3.4% at 4c and NR levels, also for Ba clusters. Both, electron correlation and relativity contract M···O bonds. Binding energies are more sensitive to the level of theory: relativistic effects reach 1.4% for Ba clusters at the 4c-DHF level and correlation effects reach 11.6% at NR level also for Ba clusters. Relativistic effects at the DHF level are larger than the corresponding PBE0 ones; this shows that correlated calculations reduce relativistic effects or both effects have opposite sign.

### 3.5.2 | Nuclear magnetic shieldings

In Table 6 we present the values of the relativistic nuclear magnetic shieldings for both Sr and Ba nuclei at different levels of theory. All shielding calculations were carried out using the dyall.c4vz basis set. This choice of basis set is justified by the results shown in section 3 of the Supporting Information as follows: the difference between the calculated  $\sigma(Ba)$  using dyall.c4vz and the largest basis set is close to 0.03% at DHF level of



**FIGURE 6** Nuclear magnetic shieldings  $\sigma(M)$  for the global minima in the 4c-relativistic potential energy surfaces for the microsolvation of  $\text{Sr}^{2+}$ ,  $\text{Ba}^{2+}$  with up to three water molecules. The speed of light was scaled to  $c = 100c_0$  to obtain non-relativistic values. The bottom panels show the total accumulation of electron density in atomic units at the bond critical points for intermolecular M...O contacts. Notice that strictly speaking, there are no associated BCPs for  $n = 0$ , however,  $\sum \rho(r_c) = 0$  is included for clarity

theory, and close to 0.02% at the relativistic PBE0 level of theory. Then, considering that calculations of shieldings with the dyall.c4vz basis set have converged and are feasible, we decided to use it for all shielding calculations along the different sets of motifs.

As it is well known,  $\sigma(M)$  depends on the number of electrons surrounding the nucleus, that is, at each  $n$ ,  $\sigma(\text{Ba}) > \sigma(\text{Sr})$ , as can be seen in Figure 6. This is the case for relativistic and non-relativistic calculations at both, HF/DHF and PBE0 levels.

Relativistic effects grow as the number of water molecules,  $n$ , that surrounds the central cation grows, but only up to 1% for both atoms from  $n = 1$  to  $n = 3$  at the DHF level; however, under DFT such differences grow up to 5% for Sr and up to 2% for Ba. This may be due to the environment, since the density of the electron cloud around those cations becomes smaller when  $n$  increases, thus reducing the magnetic shielding. The same behavior is observed for electron correlation effects in both frameworks, NR and relativistic. On the other hand, relativistic effects on  $\sigma$  are larger than electron correlation effects for the central cations (top panels of Figure 6). In this case the NR values are 11% for  $\sigma(\text{Sr})$  (26% for  $\sigma(\text{Ba})$ ) larger than the relativistic ones at DHF and PBE0 levels. Furthermore, the dependence of  $\sigma(\text{Sr})$  with  $n$  is linear for  $n = 1, 2$  but such a dependence breaks down for  $n = 3$  at the 4c-DHF, NR-HF and NR-PBE0 levels. On the other hand at the 4c-PBE0 level that dependence is still linear for  $n > 2$ . This last dependence is also observed for  $\sigma(\text{Ba})$ . When both effects depend linearly with  $n$ , relativistic and electron correlation seem to be independent each other, but this is not the case for  $\sigma(\text{Sr})$ .

As observed at the bottom of Figure 6, there is a shift of electron density upon cluster formation. We have previously shown [86] that the relativistic effects on magnetic shieldings increase when ionicity increases, in other words, when a neutral atom becomes ionic, the percentage of relativistic effect on the ion is larger than that percentage for the neutral atom. It is seen from the same Figure 6 that  $\sigma(\text{Ba}) > \sigma(\text{Sr})$ , nonetheless, the presence of water molecules surrounding the cations has a larger effect on the nuclear magnetic shieldings at Sr than at Ba. Indeed, solvent effects produce a reduction of the nuclear magnetic shielding of both cations: at the DHF level, when the number of water molecules increases up to  $n = 3$ , the shielding decreases 431 ppm for the  $\text{Sr}^{2+}$  nucleus, which represents close to 11% of the free ion shielding value; a similar reduction of 381 ppm, corresponding to 5% of the free ion shielding is seen for  $\text{Ba}^{2+}$  [87]. This is consistent with the above discussed stronger interaction energies in the Sr containing clusters. The reduction of  $\sigma$  by solvent effects in a divalent ion was reported previously for a heavier nucleus,  $\text{Hg}^{2+}$  [86].

As mentioned above, we were interested on learning about the dependence of the nuclear magnetic shieldings of microsolvated cations as a function of the number of water molecules and as a function of the identity (size) of the cation. We found that  $\sigma(M)$  decreases as the number of

water molecules in direct contact with the central cation increases. This fact must be related with the variation of the electronic density at the site of the nucleus M, which is not related to relativistic effects in our case. We observe that, when the number of water molecules increases, the electron densities at BCPs do increase, and the shielding on the M atom goes down. What seems to happen is that the electron density that is located on the region close to the M atom is shifted to the BCP as the number of water molecules increases. Most of the electron density may come from the lone pairs at the oxygen atoms, but some should also come from the cation, thus leading to the observed decrease in  $\sigma(M)$ .

## 4 | CONCLUSIONS

An intensive stochastic exploration of the PESs for the microsolvation of  $\text{Sr}^{2+}$ ,  $\text{Ba}^{2+}$  with up to six explicit water molecules is presented in this work. We investigate the problem within relativistic and non-relativistic frameworks with large enough basis sets. We assess correlation and relativistic effects in molecular geometries and binding energies by comparing DHF against PBE0 in both regimes using the non-relativistic limit by scaling the speed of light by a factor of 100. Relativistic nuclear magnetic shieldings at the central cation  $\sigma(M)$  immersed in the microsolvated environment are also discussed.

We found complex and rich energy landscapes containing a total of 46 well characterized structural motifs with many structures not reported previously in the specialized literature. Among them, a number of structures in which the formal charge in the cation is strong enough to induce dissociation of neighboring water molecules into  $\text{OH}^-$  and  $\text{H}^+$  and subsequent microsolvation of the ions. Up to six water molecules, there is a direct correlation between the number of water molecules in direct contact with the central cation and the stabilizing energy of the cluster. As a general rule, computed sequential hydration enthalpies, that is, the enthalpy involved in the  $[\text{M}(\text{H}_2\text{O})_{n-1}]^{2+} + \text{H}_2\text{O} \rightarrow [\text{M}(\text{H}_2\text{O})_n]^{2+}$  reaction are in excellent agreement with experimental results, with very low errors, no larger than 10% in one extreme case.

Relativistic effects are negligible in molecular geometries, leading to less than 1% contraction of  $\text{M}\cdots\text{O}$  distances. Binding energies are also only slightly affected by relativistic effects which in all cases increase such energies. On the other hand they are not small for nuclear magnetic shieldings. Thus relativity cannot be ignored when calculating this particular property in microsolvated cations of Sr and Ba, because of contributions of the order of 13% for  $\sigma(\text{Sr})$  and around 27% for  $\sigma(\text{Ba})$ . We point out that, counterintuitively, the nuclei of central cations are deshielded (around 10% in going from  $n=1$  to  $n=3$ ) due to microsolvation.

The formal charge introduces a chaotropic effect in the water to water hydrogen bonds, significantly increasing their strength and reducing their interaction distances.  $\text{M}\cdots\text{O}$  chemical bonding in the clusters is a considerably more complicated issue, which is heavily affected by the environment. While many  $\text{M}\cdots\text{O}$  contacts are characterized as purely ionic by QTAIM descriptors, a large number are also characterized as of intermediate character with contributions from both ionic and covalent interactions, thus transcending a simplistic view of electrostatic attraction between opposite charges. More precisely, a deshielding of both Sr, Ba nuclei, which increases with the number of water molecules, is seen as a consequence of the direct intermolecular interactions. Furthermore, this withdraw of electron density from the initially doubly charged cations is rationalized by a non-linear increase in the total electron density of the associated  $\text{M}\cdots\text{O}$  bond critical points as a function of the coordination number of M.

## ACKNOWLEDGMENTS

Partial financial support for this project from Universidad de Antioquia via “Estrategia para la sostenibilidad” is acknowledged. A. M. and G. A. acknowledge support from the Argentinian Research Council on Science and Technology, CONICET (Grant PIP 112-201301-00361), and from the Argentinian Agency for Promotion of Science and Technology, FONCYT (Grant PICT2016-2936).

## AUTHOR CONTRIBUTIONS

**Angie Velásquez:** Formal analysis; investigation; writing-original draft; writing-review & editing. **Yuly Chamorro:** Formal analysis; investigation; methodology; writing-original draft; writing-review & editing. **Alejandro Maldonado:** Formal analysis; investigation; writing-original draft; writing-review & editing. **Albeiro Restrepo:** Conceptualization; formal analysis; writing-original; writing-review and editing, funding acquisition. **Gustavo Aucar:** Conceptualization; formal analysis; writing-review and editing, funding acquisition.

## DATA AVAILABILITY STATEMENT

The data that supports the findings of this study are available within the article and its supplementary material.

## ORCID

Alejandro Maldonado  <https://orcid.org/0000-0003-3587-3736>

Gustavo Aucar  <https://orcid.org/0000-0003-2547-2330>

Albeiro Restrepo  <https://orcid.org/0000-0002-7866-7791>

## REFERENCES

- [1] C. Hadad, E. Florez, N. Acelas, G. Merino, A. Restrepo, *Int. J. Quantum Chem.* **2019**, *119*, e25766.
- [2] J. D. Gonzalez, E. Florez, J. Romero, A. Reyes, A. Restrepo, *J. Mol. Model.* **2013**, *19*, 1763.
- [3] J. Romero, A. Reyes, J. David, A. Restrepo, *Phys. Chem. Chem. Phys.* **2011**, *13*, 15264.
- [4] J. S. Rao, T. Dinadayalane, J. Leszczynski, G. N. Sastry, *J. Phys. Chem. A* **2008**, *112*, 12944.
- [5] A. Boda, S. De, S. M. Ali, S. Tulishetti, S. Khan, J. K. Singh, *J. Mol. Liq.* **2012**, *172*, 110.
- [6] S. G. Neogi, P. Chaudhury, *Indian J. Phys.* **2014**, *88*, 781.
- [7] T. S. Hofer, B. R. Randolph, B. M. Rode, *J. Phys. Chem. B* **2006**, *110*, 20409.
- [8] A. Kerridge, N. Kaltsoyannis, *Chem. A Eur. J.* **2011**, *17*, 5060.
- [9] M. Pavlov, P. E. Siegbahn, M. Sandstöm, *J. Phys. Chem. A* **1998**, *102*, 219.
- [10] B. Hartke, A. Charvat, M. Reich, B. Abel, *J. Chem. Phys.* **2002**, *116*, 3588.
- [11] E. D. Glendenning, D. Feller, *J. Phys. Chem.* **1996**, *100*, 4790.
- [12] F. Zhu, H. Zhou, C. Fang, Y. Fang, Y. Zhou, H. Liu, *Mol. Phys.* **2018**, *116*, 273.
- [13] C. W. Bauschlicher Jr., M. Sodupe, H. Partridge, *J. Chem. Phys.* **1992**, *96*, 4453.
- [14] E. Miliordos, S. S. Xantheas, In *Highlights in Theoretical Chemistry* (Eds: A. Wilson, K. Peterson, D. Woon, T. H. Dunning, Jr.). vol. 10, Springer, Berlin, Heidelberg **2015**.
- [15] M. P. Blaustein, *Am. J. Physiol. Cell Physiol.* **1977**, *232*, C165.
- [16] J. Hall, *Am. J. Physiol. Regul. Integr. Comp. Physiol.* **1986**, *250*, R960.
- [17] H. E. Corey, *Crit. Care* **2004**, *9*, 184.
- [18] O. Skøtt, *Am. J. Physiol. Regul. Integr. Comp. Physiol.* **2003**, *285*, R14.
- [19] H. Hibino, A. Inanobe, K. Furutani, S. Murakami, I. Findlay, Y. Kurachi, *Phys. Rev.* **2010**, *90*, 291.
- [20] A. Hartwig, *Mutat. Res.* **2001**, *475*, 113.
- [21] W. Yang, J. Y. Lee, M. Nowotny, *Mol. Cell* **2006**, *22*, 5.
- [22] M. Selmer, C. M. Dunham, F. V. Murphy, A. Weixlbaumer, S. Petry, A. C. Kelley, J. R. Weir, V. Ramakrishnan, *Science* **2006**, *313*, 1935.
- [23] D. J. Klein, P. B. Moore, T. A. Steitz, *RNA* **2004**, *10*, 1366.
- [24] G. Beaven, J. Parmar, G. Nash, P. Bennett, W. Gratzer, *J. Membr. Biol.* **1990**, *118*, 251.
- [25] M. Glimcher, *J. Rev. Mineral. Geochem.* **2006**, *64*, 223.
- [26] M. Brini, T. Cali, D. Ottolini, E. Carafoli, *FEBS J.* **2013**, *280*, 5385.
- [27] B. Katz, R. Miledi, *J. Physiol.* **1970**, *207*, 789.
- [28] R. Zangi, *J. Phys. Chem. B* **2010**, *114*, 643.
- [29] S. Komorovsky, M. Repisky, O. Malkina, V. Malkin, I. Ondik, M. Kaupp, *J. Chem. Phys.* **2008**, *128*, 104101.
- [30] Y. Xiao, Q. Sun, W. Liu, *Theor. Chem. Acc.* **2012**, *131*, 1080.
- [31] P. Pyykkö, *Annu. Rev. Phys. Chem.* **2012**, *63*, 45.
- [32] T. Saue, *ChemPhysChem* **2011**, *12*, 3077.
- [33] D. Peng, W. Liu, Y. Xiao, V. Cheng, L. Makin, *J. Chem. Phys.* **2007**, *127*, 104106.
- [34] K. Dyall, *J. Chem. Phys.* **2001**, *115*, 9136.
- [35] M. Reiher, A. Wolf, *Relativistic Quantum Chemistry*, 2nd ed., Wiley-VCH, Weinheim **2015**.
- [36] W. Liu, *Phys. Rep.* **2014**, *537*, 59.
- [37] Y. Xiao, W. Liu, L. Cheng, D. Peng, *J. Chem. Phys.* **2007**, *126*, 214101.
- [38] B. Simmen, E. Mátyus, M. Reiher, *J. Phys. B: At., Mol. Opt. Phys.* **2015**, *48*, 245004.
- [39] S. Komorovsky, M. Repisky, O. Malkina, V. Malkin, *J. Chem. Phys.* **2010**, *132*, 5154101.
- [40] J. Vaara, *Phys. Chem. Chem. Phys.* **2007**, *9*, 5399.
- [41] S. Moncho, J. Autschbach, *J. Chem. Theory Comput.* **2010**, *6*, 223.
- [42] F. Alkan, S. T. Holmes, R. J. Iuliucci, K. T. Mueller, C. Dybowski, *Phys. Chem. Chem. Phys.* **2016**, *18*, 18914.
- [43] G. A. Aucar, J. I. Melo, I. A. Aucar, A. F. Maldonado, *Int. J. Quantum Chem.* **2018**, *118*, e25487.
- [44] M. Repisky, S. Komorovsky, M. Kadek, L. Konecny, U. Ekström, E. Malkin, M. Kaupp, K. Ruud, O. L. Malkina, V. G. Malkin, *J. Chem. Phys.* **2020**, *152*, 184101.
- [45] G. A. Aucar, J. Oddershede, *Int. J. Quantum Chem.* **1993**, *47*, 425.
- [46] G. A. Aucar, R. H. Romero, A. F. Maldonado, *Int. Rev. Phys. Chem.* **2010**, *29*, 1.
- [47] G. Aucar, T. Saue, L. Visscher, H. A. Jensen, *J. Chem. Phys.* **1999**, *110*, 6208.
- [48] Q. Sun, W. Liu, W. Kutzelnigg, *Theor. Chem. Acc.* **2011**, *129*, 423.
- [49] M. Olejniczak, R. Bast, T. Saue, M. Pecul, *J. Chem. Phys.* **2012**, *136*, 014108.
- [50] E. Flórez, N. Acelas, C. Ibarguen, S. Mondal, J. L. Cabellos, G. Merino, A. Restrepo, *RSC Adv.* **2016**, *6*, 71913.
- [51] Y. Chamorro, E. Flórez, A. F. Maldonado, G. A. Aucar, A. Restrepo, *Int. J. Quantum Chem.* **2020**, *121*, e26571.
- [52] E. Florez, A. F. Maldonado, G. A. Aucar, J. David, A. Restrepo, *Phys. Chem. Chem. Phys.* **2016**, *18*, 1537.
- [53] J. F. Pérez, E. Florez, C. Z. Hadad, P. Fuentealba, A. Restrepo, *J. Phys. Chem. A* **2008**, *112*, 5749.
- [54] J. F. Pérez, C. Z. Hadad, A. Restrepo, *Int. J. Quantum Chem.* **2008**, *108*, 1653.
- [55] J. Pérez, A. Restrepo, *ASCEC V-02: Annealing Simulado con Energía Cuántica. Property, Development and Implementation: Grupo de Química-Física Teórica*, Instituto de Química, Universidad de Antioquia, Medellín, Colombia **2008**.
- [56] M. J. Frisch, G. W. Trucks, H. B. Schlegel, G. E. Scuseria, M. A. Robb, J. R. Cheeseman, G. Scalmani, V. Barone, B. Mennucci, G. A. Petersson, H. Nakatsuji, M. Caricato, X. Li, H. P. Hratchian, A. F. Izmaylov, J. Bloino, G. Zheng, J. L. Sonnenberg, M. Hada, M. Ehara, K. Toyota, R. Fukuda, J. Hasegawa, M. Ishida, T. Nakajima, Y. Honda, O. Kitao, H. Nakai, T. Vreven, J. A. Montgomery Jr., J. E. Peralta, F. Ogliaro, M. Bearpark, J. J. Heyd, E. Brothers, K. N. Kudin, V. N. Staroverov, R. Kobayashi, J. Normand, K. Raghavachari, A. Rendell, J. C. Burant, S. S. Iyengar, J. Tomasi, M. Cossi, N. Rega, J. M. Millam, M. Klene, J. E. Knox, J. B. Cross, V. Bakken, C. Adamo, J. Jaramillo, R. Gomperts, R. E. Stratmann, O. Yazyev, A. J. Austin, R. Cammi, C.

- Pomelli, J. W. Ochterski, R. L. Martin, K. Morokuma, V. G. Zakrzewski, G. A. Voth, P. Salvador, J. J. Dannenberg, S. Dapprich, A. D. Daniels, Ö. Farkas, J. B. Foresman, J. V. Ortiz, J. Cioslowski, D. J. Fox, *Gaussian 09 Revision E.01*, Gaussian, Inc., Wallingford, CT **2009**.
- [57] R. Bader, *Atoms in Molecules: A Quantum Theory*, Oxford University Press, Oxford **1990**.
- [58] R. F. W. Bader, *Chem. Rev.* **1991**, *91*, 893.
- [59] R. F. W. Bader, *Monatsh. Chem.* **2005**, *136*, 819.
- [60] P. Popelier, *Coord. Chem. Rev.* **2000**, *197*, 169.
- [61] P. L. Popelier, *Atoms in Molecules: An Introduction*, Prentice Hall, London **2000**.
- [62] A. Becke, *The Quantum Theory of Atoms in Molecules: From Solid State to DNA and Drug Design*, John Wiley & Sons, Weinheim **2007**.
- [63] T. Keith. AIMALL (version 19.10.12). TK Gristmill Software, Overland Park, KS **2019**, [www.aim.tkgristmill.com](http://www.aim.tkgristmill.com).
- [64] E. Espinosa, I. Alkorta, J. Elguero, E. Molins, *J. Chem. Phys.* **2002**, *117*, 5529.
- [65] D. Carl, B. K. Chatterjee, P. Armentrout, *J. Chem. Phys.* **2010**, *132*, 044303.
- [66] O. W. Wheeler, D. R. Carl, T. E. Hofstetter, P. Armentrout, *J. Phys. Chem. A* **2015**, *119*, 3800.
- [67] DIRAC, a relativistic ab initio electronic structure program, Release DIRAC17, written by L. Visscher, H. J. Aa. Jensen, R. Bast, and T. Saue, with contributions from V. Bakken, K. G. Dyall, S. Dubillard, U. Ekström, E. Eliav, T. Enevoldsen, E. Faßhauer, T. Fleig, O. Fossgaard, A. S. P. Gomes, E. D. Hedegård, T. Helgaker, J. Henriksson, M. Iliaš, Ch. R. Jacob, S. Knecht, S. Komorovský, O. Kullie, J. K. Lærdahl, C. V. Larsen, Y. S. Lee, H. S. Nataraj, M. K. Nayak, P. Norman, G. Olejniczak, J. Olsen, J. M. H. Olsen, Y. C. Park, J. K. Pedersen, M. Pernpointner, R. di Remigio, K. Ruud, P. Sałek, B. Schimmelpennig, A. Shee, J. Sikkema, A. J. Thorvaldsen, J. Thyssen, J. van Stralen, S. Villaume, O. Visser, T. Winther, and S. Yamamoto **2017**. <http://www.diracprogram.org>
- [68] K. G. Dyall, *J. Phys. Chem. A* **2009**, *113*, 12638.
- [69] A. F. Maldonado, G. A. Aucar, *Phys. Chem. Chem. Phys.* **2009**, *11*, 5615.
- [70] G. A. Aucar, A. F. Maldonado, M. D. A. Montero, T. Santa Cruz, *Int. J. Quantum Chem.* **2019**, *119*, e25722.
- [71] I. Tunell, *Inorg. Chem.* **2006**, *45*, 4811.
- [72] A. F. Maldonado, G. A. Aucar, *J. Phys. Chem. A* **2014**, *118*, 7863.
- [73] F. Ramírez, C. Hadad, D. Guerra, J. David, A. Restrepo, *Chem. Phys. Lett.* **2011**, *507*, 229.
- [74] G. Hincapié, N. Acelas, M. Castano, J. David, A. Restrepo, *J. Phys. Chem. A* **2010**, *114*, 7809.
- [75] N. Acelas, G. Hincapié, D. Guerra, J. David, A. Restrepo, *J. Chem. Phys.* **2013**, *139*, 044310.
- [76] H.-H. Limbach, P. M. Tolstoy, N. Pérez-Hernández, J. Guo, I. G. Shenderovich, G. S. Denisov, *Isr. J. Chem.* **2009**, *49*, 199.
- [77] C. J. D. van Grothuss *Ann. Chim.* **1805**, *58*, 54.
- [78] E. Parzen, *Ann. Math. Stat.* **1962**, *33*, 1065.
- [79] N. Rojas, S. Gómez, D. Guerra, A. Restrepo, *Phys. Chem. Chem. Phys.* **2020**, *22*, 13049.
- [80] P. Farfán, A. Echeverri, E. Díaz, J. D. Tapia, S. Gómez, A. Restrepo, *J. Chem. Phys.* **2017**, *147*, 044312.
- [81] N. Rojas-Valencia, C. Ibagüen, A. Restrepo, *Chem. Phys. Lett.* **2015**, *635*, 301.
- [82] I. Alkorta, I. Rozas, J. Elguero, *Struct. Chem.* **1998**, *9*, 243.
- [83] O. Knop, R. J. Boyd, S. Choi, *J. Am. Chem. Soc.* **1988**, *110*, 7299.
- [84] L. Pauling *The Nature of the Chemical Bond: And the Structure of Molecules and Crystals; An Introduction to Modern Structural Chemistry*. Oxford University Press, London **1940**.
- [85] C. Coulson, *Valence*, Oxford University Press, London **1961**.
- [86] K. Koziol, I. A. Aucar, G. A. Aucar, *J. Chem. Phys.* **2019**, *150*, 184301.
- [87] J. Roukala, A. F. Maldonado, J. Vaara, G. A. Aucar, P. Lantto, *Phys. Chem. Chem. Phys.* **2011**, *13*, 21016.

## SUPPORTING INFORMATION

Additional supporting information may be found online in the Supporting Information section at the end of this article.

**How to cite this article:** A. Velásquez, Y. Chamorro, A. Maldonado, G. Aucar, A. Restrepo, *Int J Quantum Chem* **2021**, e26753. <https://doi.org/10.1002/qua.26753>